1 Introduction

We have undertaken a systematic study to identify a sample of massive protostellar candidates. Started with a selection of sources from the IRAS-PSC2 catalogue and on the basis of observations of H_2O masers (Palla et al. 1991), ammonia lines (Molinari et al. 1996), and centimeter and submillimeter continuum (Molinari et al. 1998a, 1998b), we have selected a final sample of a dozen candidates to be precursors of UCHII regions. We have now started a pilot program to observe these objects by means of millimeter interferometry. We present the results obtained on the first source observed, IRAS 23385+6053, which we found to be an excellent candidate of a high-mass Class 0 object. The source:

- is **associated** with an H_2O maser (Palla et al. 1991), NH_3 line and submillimeter continuum emission (Molinari et al. 1996; 1998b)
- is **not associated** with centimeter continuum emission (Molinari et al. 1998a) at the VLA down to a level of ~ 0.5 mJy/beam at 6 cm.
- has $\mathbf{L}_{bol} \sim 16000\ \mathbf{L}_{\odot}$ at a kinematic distance of 4.9 kpc.

2 Observations

OVRO

The six OVRO 10.4-m dishes were used in two different configurations providing baselines in the range 15-240 m. Simultaneous observations of the 3.4mm continuum, $HCO^+(1 \rightarrow 0)$ $H^{13}CO^+(1 \rightarrow 0)$ and SiO(v=0, $2 \rightarrow 1$) rotational lines were obtained. The FWHM of the synthesized beam is $4''.1 \times 3''.5$ and the estimated flux uncertainty is less than 20%.

ISOCAM

Staring mode images in the two broad-band filters LW2 (λ_{eff}=6.75μm) and LW3 (λ_{eff}=15.0μm) were obtained with an integration time of 100s in each filter; expected 3σ sensitivity limits are 0.33 and 0.45 mJy/arcsec^2 in LW2 and LW3, respectively. The spatial resolution is $2''.2$ and $5''$ at the two wavelength respectively (limited by diffraction) with a $3''$ PFOV, and the absolute calibration is expected to be accurate within 20%.

3 The HCO^+/mm Core

- The HCO^+ line and the 3.4 mm continuum arise from the central region where the 15 μm continuum is faintest. No millimeter emission is detected towards the bright spots seen on the 15 μm image.

- The 3.4 mm continuum the core is compact with a fainter SE elongation and an asymmetry north of the central peak. The integrated flux density is 19 mJy in a deconvolved area of $4''.5 \times 3''.6$ **(radius $\sim$ 0.048 pc)**. The peak position of the 3.4 mm peak is $\alpha(1950) = 23^h : 38^m : 31^s.4$, $\delta(1950) = +60° : 53' : 50''$.

- 15 μm fluxes at the position of the 3.4 mm core, $\sim$1 mJy/arcsec^2 are similar to those in the southern portion of the CAM field, suggesting that it is due to faint foreground emission; its rms is $\sim$0.15 mJy/arcsec^2 (similar rms are obtained for the 6.75 μm image. We thus conclude that **no 15 μm counterpart is detected at the position of the 3.4 mm core to a 3σ level of** $\sim$ 0.45 mJy/arcsec^2 (e.g. $\sim$ 6 **mJy** on the deconvolved area of the 3.4 mm core).

- **The bright 15 μm emission seen in Fig. 1**, which is not directly related to the millimeter core, **is responsible for the IRAS 12 and 25μm flux densities**; indeed the latter (5.05 and 17.8 Jy, respectively) are compatible with the CAM 7 and 15 μm flux integrated over all the bright emission visible on Fig. 1 ($\sim$4.8 and 9.3 Jy respectively, on an area of 320 pixels or 6.8×10^{-8} sterad), while they lie more than 3 orders of magnitude above the flux density limits of the core estimated in the CAM images (see previous point).

- **The millimeter core is the only source contributing significantly at 60 and 100 μm**. Indeed: 1) at millimeter wavelengths, the core is compact and no discrete or diffuse continuum emission is detected at either OVRO or with the JCMT; 2) a power law extrapolation of the 6.75, 12, 15 and 25 μm flux densities observed from the bright emission areas seen in the CAM image to longer wavelengths, leads to flux densities at 60 and 100 μm $\lesssim$ 5% of the observed values.

4 The SED of the HCO^+/mm Core

- The millimeter continuum emission is interpreted as being due to dust thermal emission with no contribution from free-free emission since the source is undetected at centimeter wavelengths. The OVRO flux density is consistent with those from JCMT (Molinari et al. 1998b) indicating that no significant diffuse millimeter emission has been missed by the interferometer.

- The dotted line on Fig. 2 is a fit to the data, obtained adopting a spherical dust envelope model where density and temperature vary according to radial power laws with exponents -0.5 and -0.4 respectively. The density and temperature at the external radius ($r_{core} \simeq$ 0.048pc) are $7\times10^6 cm^{-2}$ and 40 K. The opacity is $\kappa_\nu(cm^2\,g^{-1})=0.005\,(\nu(GHz)/230.6)^{1.9}$ (Preibisch et al. 1993).

- We compute the bolometric luminosity of the source by integrating the data with a power law interpolation scheme, excluding the IRAS 12 and 25 μm flux densities and using the CAM upper limit at 15 μm. At the adopted distance of 4.9 kpc, we find $\mathbf{L}_{bol} \simeq 1.6 \times 10^4\ \mathbf{L}_\odot$.

Assuming optically thin emission at 3.4 mm and a gas to dust ratio of 100 by mass, we estimate a mass of $\sim$ **370** $\mathbf{M_\odot}$ and a mean $\mathbf{H_2}$ **column density of** $\sim 2 \times 10^{24}$ $\mathbf{cm^{-2}}$ for the core. The latter value corresponds to a visual extinction $\mathbf{A_V} \sim 2000$.

5 The Molecular Outflow

We show in Fig. 3 the maps of the HCO^+ (left panel) and SiO (right panel) emission integrated over the blue (from -63 to -53 km s^{-1}) and the red (from -47 to -37 km s^{-1}) wings. The cross represents the position of the HCO^+/3.4mm core.

- We detect an **outflow centered on the continuum source and with axis oriented nearly perpendicular to the plane of the sky**. The lobes are barely resolved; their position relative to each other, i.e. their degree of overlap, suggests that the inclination of its axis can be no more than 30° with respect to the line of sight (Cabrit & Bertout 1986; 1990). **The non-detection of the central source at 15 μm suggests an upper limit for the lobes extension of $\mathbf{r}_{lobe} \leq \mathbf{r}_{core}$=0.048 pc.**

- Outflow parameters for SiO and HCO^+ were estimated in LTE and optically thin approximations. Abundances of 10^{-9} relative to H_2 and an excitation temperature of 30 K were adopted for both HCO^+ and SiO (as deduced from the peak brightness temperature of $HCO^+(1 \rightarrow 0)$ line.

- The flow mechanical power and mass loss rate are high compared to values characterising outflows powered by low-mass protostars (e.g. Fukui et al. 1993), but in good agreement with flows from high-mass young stellar objects (Shepherd & Churchwell 1996). However, the dynamical timescale is similar to values found for the youngest outflows around low-mass Class 0 objects (e.g. André et al. 1993; Bontemps et al. 1996).

6 IRAS 23385+6053: A Massive Class 0 Object

- The source has not been detected at 6 and 2 cm with the VLA with 3σ sensitivity limits of $\sim$0.5 and $\sim$0.8 mJy/beam respectively (Molinari et al. 1998a), implying that an HII region, if present, must be optically thick and very compact ($r_{HII} \lesssim 100$ AU). A very efficient mechanism that can squelch the expanding HII region is accretion; for a B0 star (which has a comparable luminosity to our source), the accretion rate needed (4×10^{-6} $M_\odot$/yr; see e.g. Walmsley 1995) is modest.

- An alternative scenario is that there is no HII region because IRAS 23385+6053 has not yet reached the ZAMS. In such a case, we assume that the observed bolometric luminosity is due to accretion onto a protostellar core with accretion luminosity expressed as $L_{acc} = 3.14 \times 10^4$ $L_\odot$ $(M_\star/M_\odot)$ $(R_\odot/R_\star)$ $(\dot{M}/10^{-3})$. We also use the mass-radius relation of Stahler, Palla & Salpeter (1986), $R_\star = 27.2\times$ $R_\odot$ $(M_\star/M_\odot)^{0.27}$ $(\dot{M}/10^{-3})^{0.41}$. Since L_{acc} is known, we can use these two equations to derive the protostellar mass $M_\star$ as a function of the accretion rate.

For an accretion rate $\dot{M} \sim 10^{-3}$ $M_\odot$/yr, which is expected if the outflow is driven by infall (e.g. Shu et al. 1988), we obtain a value of $M_\star$=39 $M_\odot$, implying that the embedded IRAS source is a massive protostar.

Independent of which of these two alternatives is correct, this source is evidently massive and extremely young.

IRAS 23385+6053 falls within the criteria with which André et al. 1993) identify a *bona fide* protostar (a Class 0 object): it is undetected in the mid-IR ($\lambda < 15\mu$m); it has $L_{submm}/L_{bol} \geq 5 \times 10^{-3}$ (where L_{submm} is obtained by integrating longward of 350μm); it has $M_{env}/M_\star \gg 1$. The very short dynamical timescale ($\lesssim$ 7000 yrs) of the associated compact molecular outflow is also compatible with values found for outflows around low-mass Class 0 objects. Based on the evidence presented here, **we propose IRAS 23385+6053 as a prototype high-mass Class 0 object**.

References

André, P., Ward-Thompson, D., & Barsony, M. 1993, ApJ, 406, 122
Bontemps, S., André, P., Tereby, S., Cabrit, S. 1996, A&A, 311, 858
Brand, J., & Blitz, L. 1993, A&A, 275, 67
Fukui, Y., Iwata, T., Mizuno, A., Bally, J., & Lane, A. P. 1993, Protostars & Planets III, p. 603
Habing, H. J., & Israel, F. P. 1979, Ann. Rev. Astron. Astroph., 17, 345
Molinari, S., Brand, J., Cesaroni, R., & Palla, F. 1996, A&A, 308, 573
Molinari, S., Brand, J., Cesaroni, R., Palla, F., & Palumbo, G.G.C. 1998a, A&A, in press
Molinari, S., Brand, J., Cesaroni, R., Palla, F. 1998b, in preparation
Palla, F., Brand, J., Cesaroni, R., Comoretto, G., & Felli, M. 1991, A&A, 246, 249
Preibisch, Th., Ossenkopf, V., Yorke, H.W., & Henning, Th. 1993, A&A, 279, 577
Shu, F. H., Lizano, S., Ruden, S. P., & Najita, J. 1988, ApJL, 328, L19
Shepherd, D. S. & Churchwell, E. 1996, ApJ, 457, 267
Stahler, S. W., Palla, F., & Salpeter, E. E. 1986, ApJ, 302, 590
Walmsley, C. M. 1995, Rev. Mex. Astron. Astrof., Series de Conferencias, 1, 137

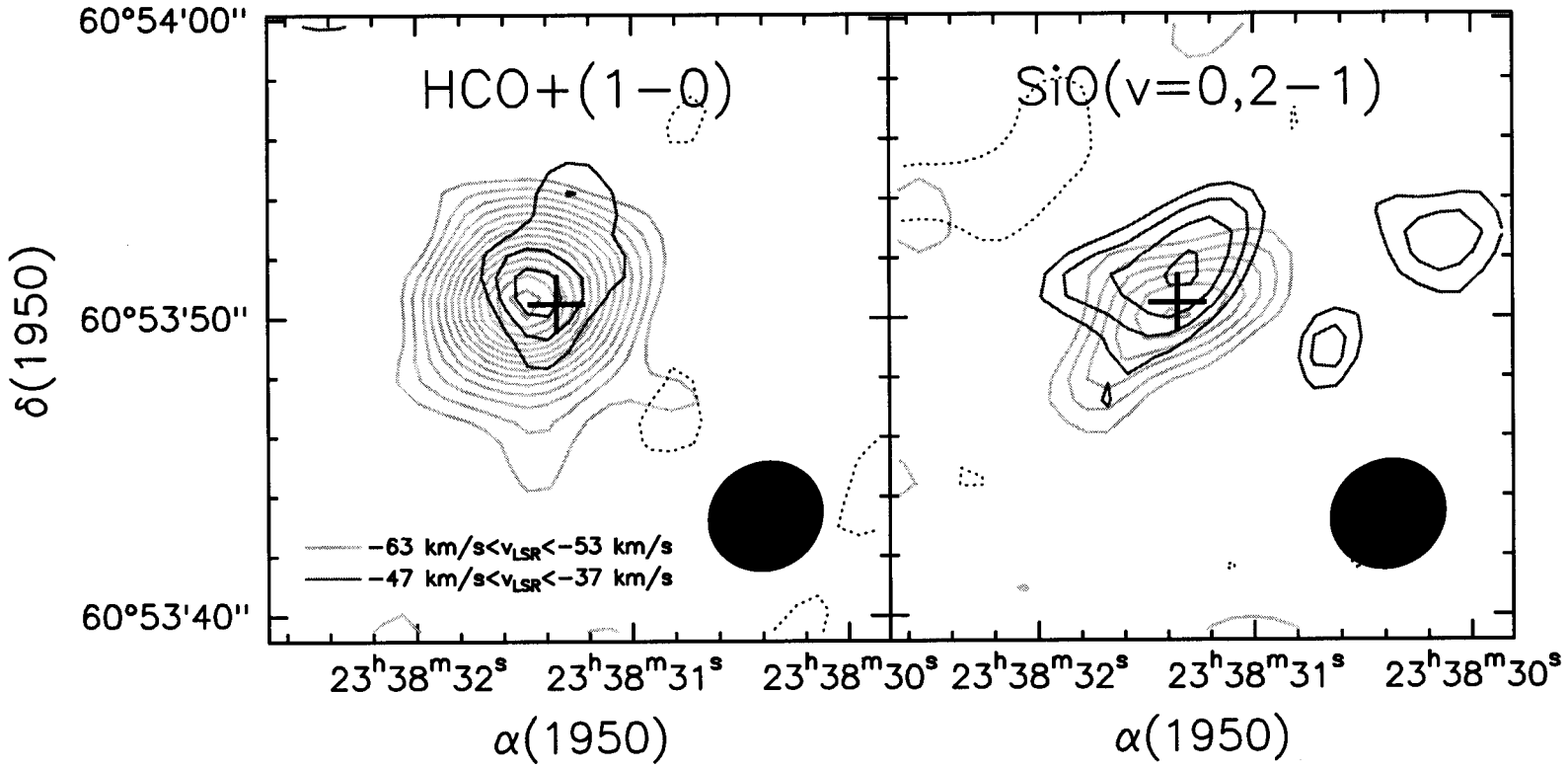
60°54'00"
60°53'50"
60°53'40"
δ(1950)
HCO+(1−0)
SiO(v=0,2−1)
−63 km/s<v_LSR<−53 km/s
−47 km/s<v_LSR<−37 km/s
23h38m32s
23h38m31s
23h38m30s
α(1950)

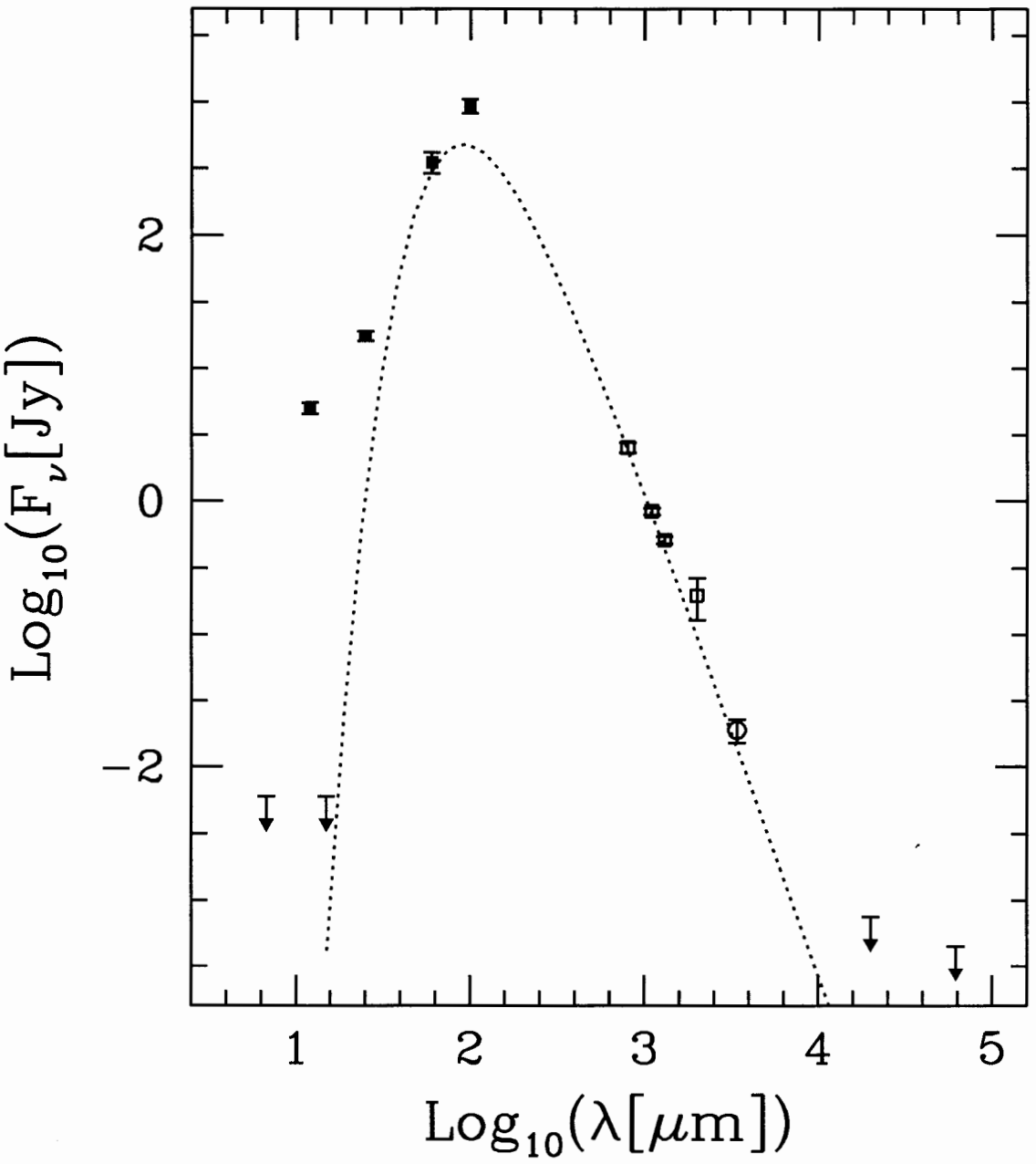

Spectral energy distribution of the IRAS 23385+6053 core. Filled and open squares are the IRAS and JCMT flux densities, respectively. The open circle is the OVRO 3.4 mm flux density. The upper limits at 2 and 6 cm are from the VLA measurements of Molinari et al. 1998a); the upper limits at 6.75 and 15μm are from the ISOCAM observations. The dotted line shows a greybody fit with $\kappa_\nu \propto \nu^{1.7}$ and T= 40 K.

Table 1. Outflow Parameters

Parameter	$HCO^+(1 \rightarrow 0)$ Blue	SiO(v=0, $2 \rightarrow 1$) Blue+Red
$N_{total}(H_2)(cm^{-2})$	7.5×10^{22}	1.4×10^{23}
$M_{total}(H_2)(M_\odot)$	10.6	19.6
$P = \sum_i M_i v_i$ ($M_\odot$km s^{-1})	66.6	159.6
$E=\frac{1}{2}\sum_i M_i v_i^2$(ergs)	4.7×10^{45}	1.4×10^{46}
$< \tau_{dyn} >$ (yrs)	7300	5600
$\dot{M}(M_\odot/yrs)$	1.5×10^{-3}	3.5×10^{-3}
$\dot{P} = P/\tau_{dyn}$	9×10^{-3}	2.8×10^{-2}
$L = E/\tau_{dyn}$ ($L_\odot$)	5.4	21.6

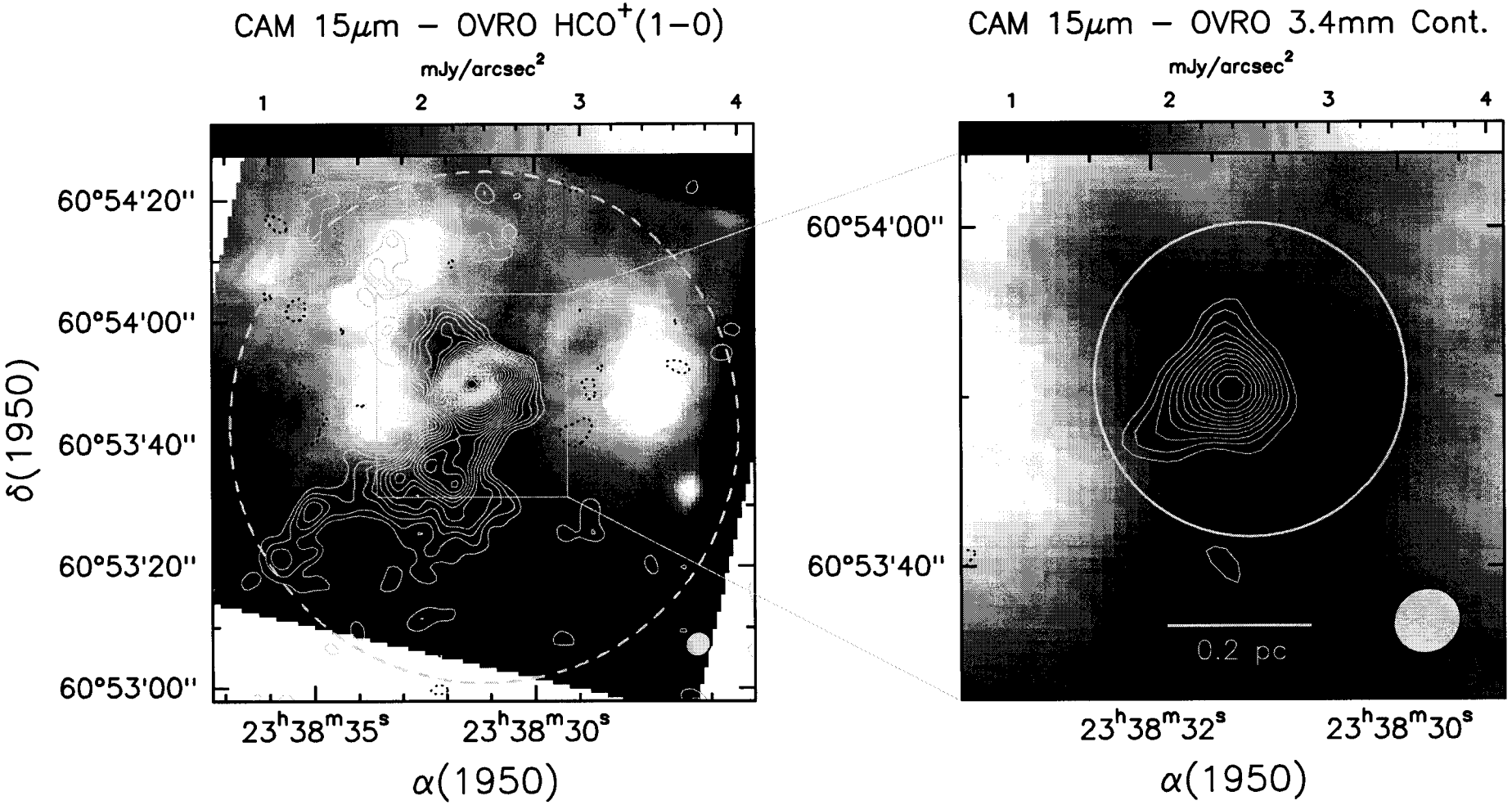
CAM 15μm – OVRO HCO+(1–0)
mJy/arcsec2
1
2
3
4
60°54'20"
60°54'00"
60°53'40"
60°53'20"
60°53'00"
δ(1950)
23h38m35s
23h38m30s
α(1950)
CAM 15μm – OVRO 3.4mm Cont.
mJy/arcsec2
1
2
3
4
60°54'00"
60°53'40"
0.2 pc
23h38m32s
23h38m30s
α(1950)